Dynamics of a truncated prion protein, PrP(113–231), from ^{15}N NMR relaxation: Order parameters calculated and slow conformational fluctuations localized to a distinct region

Denis B. D. O'Sullivan,[1] Christopher E. Jones,[1] Salama R. Abdelraheim,[2] Marcus W. Brazier,[2] Harold Toms,[1] David R. Brown,[2] and John H. Viles[1]*

[1]School of Biological and Chemical Sciences, Queen Mary University of London, London E1 4NS, United Kingdom
[2]Department of Biology and Biochemistry, University of Bath, Bath BA2 7AY, United Kingdom

Received 24 June 2008; Revised 2 October 2008; Accepted 30 October 2008
DOI: 10.1002/pro.44
Published online 29 December 2008 proteinscience.org

Abstract: Prion diseases are associated with the misfolding of the prion protein (PrP^C) from a largely α-helical isoform to a β-sheet rich oligomer (PrP^{Sc}). Flexibility of the polypeptide could contribute to the ability of PrP^C to undergo the conformational rearrangement during PrP^C–PrP^{Sc} interactions, which then leads to the misfolded isoform. We have therefore examined the molecular motions of mouse PrP^C, residues 113–231, in solution, using ^{15}N NMR relaxation measurements. A truncated fragment has been used to eliminate the effect of the 90-residue unstructured tail of PrP^C so the dynamics of the structured domain can be studied in isolation. ^{15}N longitudinal (T_1) and transverse relaxation (T_2) times as well as the proton-nitrogen nuclear Overhauser effects have been used to calculate the spectral density at three frequencies, 0, ω_N, and $0.87\omega_H$. Spectral densities at each residue indicate various time-scale motions of the main-chain. Even within the structured domain of PrP^C, a diverse range of motions are observed. We find that removal of the tail increases T_2 relaxation times significantly indicating that the tail is responsible for shortening of T_2 times in full-length PrP^C. The truncated fragment of PrP has facilitated the determination of meaningful order parameters (S^2) from the relaxation data and shows for the first time that all three helices in PrP^C have similar rigidity. Slow conformational fluctuations of mouse PrP^C are localized to a distinct region that involves residues 171 and 172. Interestingly, residues 170–175 have been identified as a segment within PrP that will form a steric zipper, believed to be the fundamental amyloid unit. The flexibility within these residues could facilitate the PrP^C–PrP^{Sc} recognition process during fibril elongation.

Keywords: PrP; structure; misfolding; backbone; intermediate; TSE; BSE; CJD

Abbreviations: BSE, bovine spongiform encephalopathy; CJD, Creutzfeldt-Jacob disease; GPI, glycosyl-phosphatidylinositol; huPrP, human PrP; mPrP, mouse PrP; PrP, prion protein; PrP^C, cellular isoform of PrP; PrP^{Sc}, scrapie isoform of PrP; SHaPrP, Syrian hamster PrP.

Additional Supporting Information may be found in the online version of this article.

O' Sullivan and Jones have contributed equally to this article.

Christopher E. Jones's current address is Center for Metals in Biology, School of Molecular and Microbial Sciences and The Queensland Brain Institute, The University of Queensland, Brisbane 4072, Australia.

Grant sponsor: BBSRC.

*Correspondence to: John H. Viles, School of Biological and Chemical Sciences, Queen Mary University of London, London E1 4NS, United Kingdom. E-mail: j.viles@qmul.ac.uk

Published by Wiley-Blackwell. © 2008 The Protein Society

Introduction

Transmissible spongiform encephalopathies or prion diseases are a group of fatal neurodegenerative disease that can be sporadic, inherited, or acquired. The infectious agent of these diseases is devoid of nucleic acid and is almost entirely composed of the prion protein, PrP^{Sc}, which is a misfolded form of a cellular prion protein PrP^{C}.[1] Recombinant prion protein has now been shown to be capable of propagating prion disease.[2] It is yet to be established what structural relationship small toxic replicating oligomeric species have with the more mature amyloid fibers.[3] It is clear the structure, flexibility, and stability of native PrP^{C} as well as folding intermediates of PrP are of significant interest to those studying the mechanism of prion misfolding and replication.

Post-translational processing of mammalian prion protein typically results in a ~208 residue glycoprotein that possesses two N-glycosylation sites and one disulfide bridge. Mature PrP^{C} is then tethered to the cell surface via a glycosyl-phosphatidylinositol anchor at the C-terminus.[1] Three dimensional NMR solution structures of non-glycosolated PrP^{C} from a number of mammalian species have been determined, including mouse,[4] Syrian hamster,[5–7] human,[8] bovine,[9] cats, dogs, pigs, sheep, chicken, turtles, frogs, and elk.[10–12] There has been some recent progress in defining the molecular architecture of prion amyloid fibers.[13,14]

The mammalian prion proteins have a high homology at the sequence and structural level. All mammalian PrP^{C} studied consist of two structurally distinct domains. The N-terminal domain (residues 23–120) is highly disordered[15] and is notable for its ability to bind Cu^{2+} ions.[16–21] The N-terminus contains a highly conserved octa-repeating sequence, PHGGGWGQ between residues 57 and 90. The flexible N-terminal tail of PrP^{C} has shown some ordering at a lower pH of 4.[22] The C-terminal domain (residues 126–231) is predominantly helical, containing 3 α-helices as well as two short anti-parallel β-strands. For mouse, PrP^{C} helix A, B, and C include residues 144–154, 175–193, and 200–219, respectively,[4,7] and for the β-sheet residues 128–131 and 161–164.[4,7]

The process of prion propagation to form amyloids has been described as a nucleation or template-assisted process, via an intermediate, PrP*. The native form of PrP is readily formed between pH 5 and 7, whereas amyloid fibers are favored under neutral pH, moderately denaturing conditions and agitation.[23] The third well characterized form of PrP is a soluble oligomeric species favored at low pH (~4) under mild denaturing conditions with a high salt content.[24–28] CD indicates this low pH oligomer has a high β-sheet content, and solution NMR studies have shown that the N-terminal tail retains its mobility in this oligomeric form.[28]

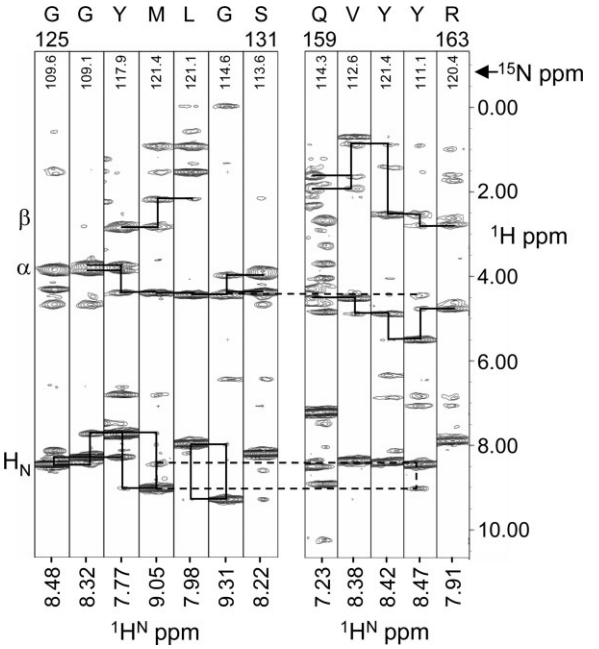

Figure 1. Series of strips from ^{1}H-$^{1}H_{N}$ slices of the 3D ^{15}N NOESY-HSQC collected at 600 MHz (^{1}H) and 30°C. Each strip corresponds to a single residue in the two-stranded β-sheet, β1 (G125–S131), and β2 (Q159–R163). Solid lines connect sequential residues, dashed lines highlight connections occurring between the strands. The assignments are shown at the top of each strip.

^{15}N NMR relaxation measurements are an unique method for probing the main-chain motions of proteins on a per-residue basis.[29,30] Slow conformational fluctuations on a milli-to-microsecond time-scale can highlight regions of PrP^{C} that sample alternative main-chain conformations. These flexible regions could facilitate protein–protein docking. ^{15}N relaxation measurements have previously been reported for full-length PrP(29–231)[15] and the 90–231 fragment.[15,31,32] However, attempts to obtain order parameters (S^2) for each NH-bond vector have been unsuccessful for the majority of residues in helix B and C for these PrP^{C} constructs.[15] These fragments contain a significant amount of the unstructured tail. This long tail, residues 23–120, may have a profound influence of the relaxation behavior of the structured C-terminal domain of PrP^{C}. Thus, the aim of this study was to use a truncated version of PrP^{C}, residues 113–231, that contains almost exclusively the structured domain of PrP^{C}. The PrP(113–231) construct was chosen because this fragment is found to occur in vivo.[33] This shorter fragment will not have its dynamics dictated by the unstructured tail and will facilitate a more detailed analysis of per-residue motions of the structured core of PrP^{C}.

Results

Assignments of mouse PrP(112–231)

The protein fragment of mouse PrP(113–231) gives well resolved ^{15}N-HSQC spectra. Assignment of the

a) MGAAAAGAVV$_{121}$ GGLGGYMLGS$_{131}$ AMSRPMIHFG$_{141}$ NDWEDRYYRE$_{151}$
NMYRYPNQVY$_{161}$ YRPVDQYSNQ$_{171}$ NNFVHDCVNI$_{181}$ TIKQHTVTTT$_{191}$
TKGENFTETD$_{201}$ VKMMERVVEQ$_{211}$ MCVTQYQKES$_{221}$ QAYYDGRRSS$_{231}$
LEHHHHHH$_{239}$

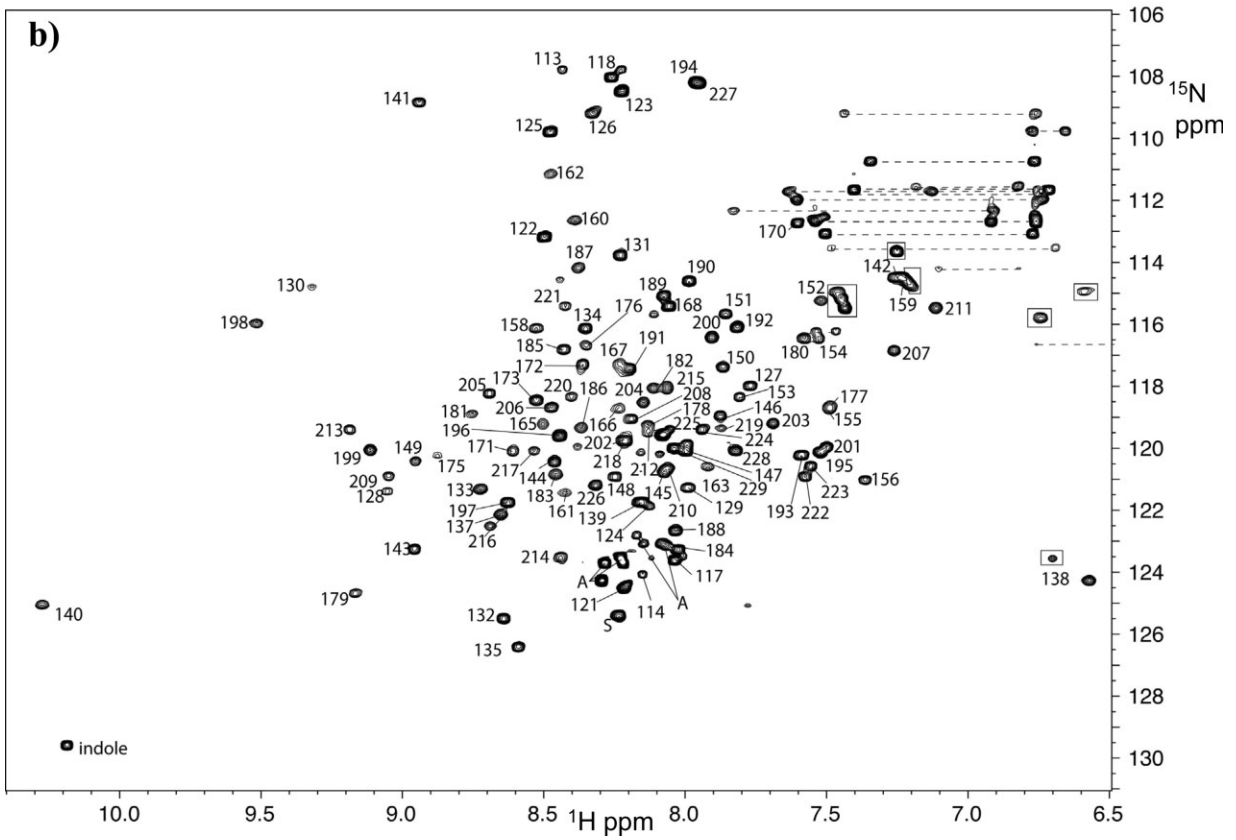

Figure 2. ^{15}N HSQC assignments for mPrP(113–231). **(a)**. Mouse PrP sequence of the C-terminal domain used in this study. **(b)** Annotated ^{15}N HSQC spectrum. Numbering relates to the sequence in (a). The C-terminal His-tag (232–239) is unassigned. Dashed lines connect side chains of unassigned Q and N sidechains. Boxes highlight folded arginine side-chain amine groups ($w_1 = w_{1,app}$ – 30 ppm). The "indole" peak is from Trp 144. The A and S are Ser and Ala residues at the N- and C-terminus.

amide resonances was completed using 3D ^{15}N HSQC-NOESY and TOCSY data. A strip-plot of the ^{15}N HSQC-NOESY spectrum is shown in Figure 1 for the region of PrP^{C} containing the short stretch of anti-parallel β-sheet. Sequential and cross-strand NOEs are indicated. Although there is strong cross-strand H_N-H_N and H_α-H_N NOEs observed between M128 and Y162 and L129 and Y162, respectively, other cross-strand diagnostic NOEs are very weak. Similarly, sequential NH-NH and αH-NH are shown (Supp. Fig. S1) for a representative stretch of α-helix, between residues 171 and 182. Consistent with other PrP^{C} structures our construct contains three α-helices and a short, two-stranded β-sheet. Helical boundaries are as follows: helix A, D143 – N152; helix B, N171 – K193; helix C, E199 – Y225, based on the observation of characteristic NOEs. Helical boundaries defined by the published mouse PrP structure are more conservatively reported as follows; 144–154, 175–193, and 200–219.[7] Although it is unnecessary in our case to solve a complete 3D structure, NOEs between secondary structure elements ensures their correct orientation in space. For instance, NOEs observed in R163 may originate from I181 and place the β-sheet adjacent to helix B. The majority of non-sequential NOEs were not assigned.

Amide main-chain assignments are indicated for the ^{15}N-HSQC shown in Figure 2, together with the mouse PrP primary sequence. All but eight main-chain amides have been assigned. Unassigned residues include: A115; A116; A119; and V120 from the N-terminus, as well as S169, F174, S230, and S231. The assignment process has been aided by backbone assignment reported for a number of other mammalian PrP's including, hamster, human, and bovine which have high sequence homology with mouse PrP.[12] TOCSY cross-peaks and NOEs allowing sequential assignment of residues forming a loop (residues 166–170) between β–sheet S2 and α–helix B are very weak (D166, Q167, Y168, N170) or missing (S169) and assignments for these residues are only tentative. Residues 166–170 were not used in detailed relaxation

analysis because of spectral overlap for these residues in the ^{15}N-HSQC.

^{15}N relaxation measurements

To gain insight into the motion of the backbone of PrP in solution ^{15}N longitudinal (T_1) and transverse (T_2) relaxation times as well as ^{15}N heteronuclear NOEs were measured at 600 MHz proton frequency for the truncated structured domain of mouse PrP residues (113–231). From a possible total of 115 main-chain amides (118 minus three prolines), we found 83 residues sufficiently dispersed to warrant relaxation analysis on a per-residue basis. In addition to eight unassigned amides, 24 more residues were not adequately resolved to permit full relaxation analysis. The residues not included in the analysis were: 115, 116, 119, 120, 122, 124, 139, 142, 145, 147, 155, 159, 166–170, 174, 177, 179, 184, 194, 195, 201, 202, 210, 212, 218, 225, 227, 230, and 231.

The R_1 ($1/T_1$) and R_2 ($1/T_2$) relaxation rates and heteronuclear NOEs for mPrP(113–231) are shown in Figure 3. The ^{15}N heteronuclear NOE values for helix A, B, and C are very similar, with values between 0.75 and 0.85. There is a dip in ^{15}N heteronuclear NOEs for the N- and C-terminus and residues between 190 and 197. Residues before 123 give negative heteronuclear NOEs indicating high mobility of the main-chain. The R_1 values are largely invariant for the bulk of the residues with typical relaxation rates between 1.3 and 1.6 s^{-1} apart from six residues at the N-terminus, which exhibit reduced R_1 rates. The R_1 values for residues in Helix C are generally lower than in the other two helices. R_2 values show the largest range of variation with mean R_2 values for helix A at 11.2 s^{-1}, which are consistently less than residues in helix B and C with mean R_2 rates of 12.1 s^{-1} and 13.5 s^{-1}, respectively. Following the trends in heteronuclear NOE values, R_2 rates are reduced for the N- and C-terminus and residues between 188 and 198. In addition, eight residues produce distinctly large R_2 rates when compared with the rest of the protein: G130, 16.3 s^{-1}; V165, 20.3 s^{-1}; Q171, 16.5 s^{-1}; N172, 16.5 s^{-1}; Q216, 15.2 s^{-1}; Y217, 15.1 s^{-1}; E220, 15.3 s^{-1}; and S221, 15.9 s^{-1}. The latter four residues are within helix C and are appreciably larger than the mean R_2 rate for helix C of 13.5 s^{-1}.

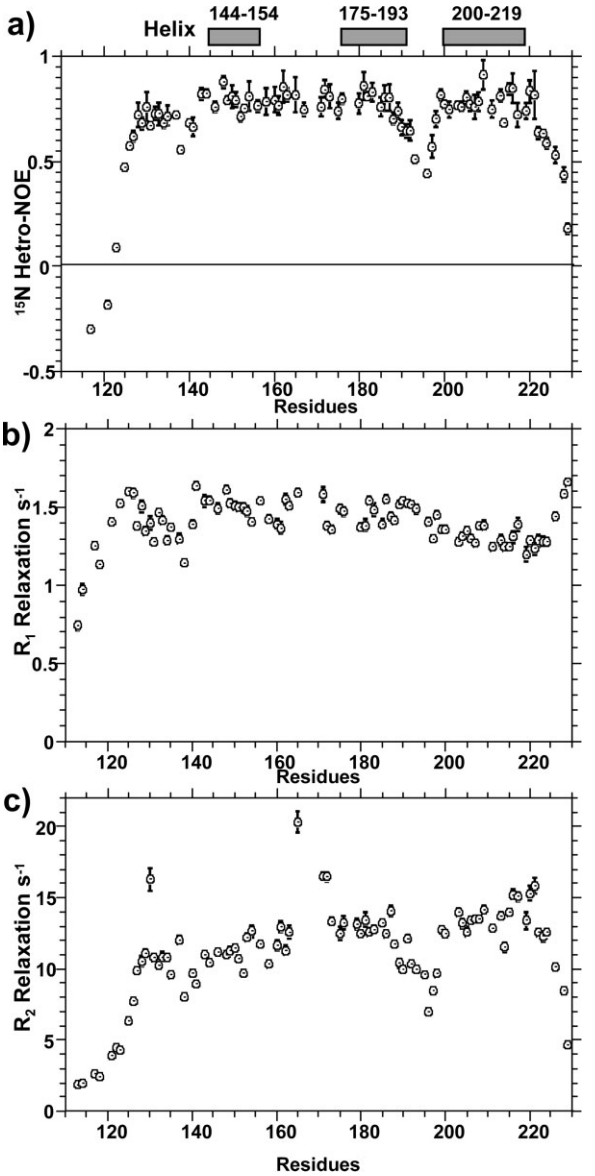

Figure 3. Relaxation data for mPrP(113–231). **(a)** Heteronuclear NOE and the relaxation rates, **(b)** R_1 ($=1/T_1$), and **(c)** R_2 ($=1/T_2$) determined at 600 MHz. Sample conditions: 30°C; pH 5.3; 20 m*M* acetate buffer.

Reduced spectral densities

J(0.87ω_H). The reduced spectral density function, J(ω), provides insights into the motion of the NH bond vector at three frequencies, zero, ω_N, and $0.87\omega_H$.[34,35] Spectra densities at these three frequencies are shown in Figure 4 on a per-residue-basis. The high frequency spectral densities J($0.87\omega_H$) are particularly useful in indicating fast pico-second motions typically observed in flexible regions of proteins. These are often associated with rapid hydrogen-bond rearrangements. J($0.87\omega_H$) spectra densities have been mapped on to the structure of PrP^C (see Supp. Fig. S2). It is clear that large J($0.87\omega_H$) are localized to the N- and C-termini of PrP(113–231), residues 113–127, and 222–231 and a loop region between helix B and C, residues 190–197. Much of the rest of the structured domain shows little fast pico-second time-scale motions. The extended polypeptide between helix A and β-strand two lacks the fast motions and has comparable J($0.87\omega_H$) to all three helixes. In addition, residues within and close to the short anti-parallel β strand-1 (residues 128–131) and strand-2 (residues 161–164) do not exhibit fast pico-second time-scale motions. It should be noted that J($0.87\omega_H$) and J(ω_N) are calculated independently of R_2 values and are

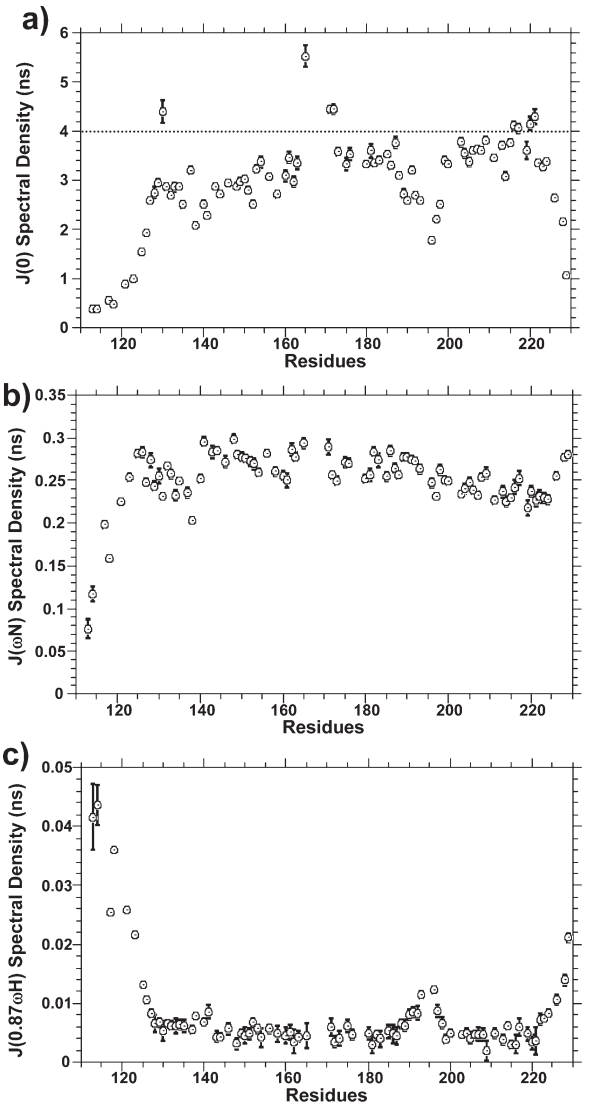

Figure 4. Reduced spectral density functions: **(a)** J(0), **(b)** $J(\omega_N)$, and **(c)** $J(0.87\omega_H)$ for mPrP(113–231) at 600 MHz. The high frequency spectral densities, $J(0.87\omega_H)$, indicate fast pico-second motions typically observed in flexible regions of proteins. J(0) indicates sub-nanosecond flexibility of the NH bond vector, the smaller the value of J(0) the greater the flexibility. Uncharacteristically large J(0) indicate residues with slow conformational fluctuations. Sample conditions: 30°C; pH 5.3; 20 m*M* acetate buffer.

therefore not influenced by slow R_{ex} milli-second to micro-second motions.

J(ω$_N$). For small proteins, $J(\omega_N)$ will decrease with increased internal flexibility. As the protein size increases this effect becomes less apparent, and for very large proteins the effect is reversed and $J(\omega_N)$ will increase with increased flexibility.[29] For PrP(113–231), a relatively small protein fragment, the flexible N-terminal residues, between 113 and 125, exhibit a reduction in $J(\omega_N)$. A reduction in $J(\omega_N)$ spectral densities relative to the bulk of the protein is not apparent for the C-terminal residues. Residues in helix C (residues 200–219 with helical character up to residue 225) show a very slight reduction in $J(\omega_N)$ spectral densities. However, helix C does not exhibit increased flexibility according to both $J(0.87\omega_H)$ and J(0) spectral densities. This reduction in $J(\omega_N)$ reflects anisotropic tumbling of PrP^C. As discussed later, N—H bond vectors in helix C are aligned with the long axis of the protein and therefore have a longer rotational diffusion time relative to helix A and B.

J(0). Assuming there are no internal motions, the spectral density function J(0) is equal to $2/5\ \tau_m$, where τ_m is the rotational correlation time. A value for J(0) less than $2/5\tau_m$ indicates internal flexibility of the NH bond; the smaller the value of J(0) the greater the sub-nanosecond flexibility of the NH bond vector.[29] There is a good deal of variation of the J(0) spectral densities. Residues in the three helices show some of the largest J(0) spectral density although there is some variation in the values, with helix A giving mean values of 3.0 ns, whereas helix B and C produce larger values for J(0) of 3.2 ns and 3.6 ns, respectively. Mirroring the $J(0.87\omega_H)$ spectral densities residues from the N- and C-termini and a loop region between helix B and C show a marked reduction in J(0) spectral densities also suggesting increased flexibility of the NH bond vector.

R$_{ex}$ motions. In addition to sub-nanosecond flexibility of the NH bond vector, slow micro- to millisecond motions can also be reflected in J(0) spectral densities, as an increase in J(0) values. The slow ms-μs (R_{ex}) motions have no effect on $J(\omega_N)$ or $J(\omega_H)$ spectral densities and so may be used to isolate these motions observed in the J(0) spectral densities. Eight residues can be identified as having J(0) spectral densities significantly greater than the bulk of the protein with J(0) greater than 4 ns, shown in Figure 4. The cutoff of 4.0 ns was set as two standard deviations greater then the mean J(0) value for helix C. The mean J(0) for helix C (residues 200–215) is 3.56 ns with a standard deviation of 0.22 ns. These eight residues do not exhibit distinct $J(\omega_N)$ or $J(\omega_H)$ spectral densities suggesting that the large J(0) values are because of exchange (R_{ex}) motions on a milli -microsecond time scale. Typically, the slow motions that cause exchange broadening are due to large segmental rearrangements rather than single H-bond rearrangements. Interestingly, four of these residues are within or close to the anti-parallel β-sheet. The J(0) spectral densities for these four residues are as follows: G130, 4.4 ± 0.2 ns; V165, 5.5 ± 0.2 ns; Q171, 4.5 ± 0.1 ns; and N172, 4.5 ± 0.1 ns. Neighboring residues 129 and 131 are resolved (in the ^{15}N HSQC spectra, Fig. 2) as are residues from the other side of the anti-parallel β-sheet, in particular, residues 160–163, whereas residue 164 is a proline. These residues do not show significantly distinct J(0) from the bulk of the protein. In

addition, four other amides exhibit J(0) spectral densities greater than 4.0 ns and are located at the end of helix C. These residues have larger J(0) spectral densities (two standard deviations from the mean) than the other residues within helix-C. These four residues Q216, Y217, E220, and S221 represent a continuous face on the C-terminal end of helix-C. Residues in the loop between β-strand 2 and helix B (166–170) may also exhibit R_{ex} motions similar to that observed for V165, Q171, and N172. It has not been possible to assign this loop (166–170) because of a lack of adequate TOCSY and NOESY data combined with spectral overlap, consequently a detailed relaxation analysis of these residues has not been possible. However, weak or missing TOCSY and NOE peaks for these residues hint at exchange broadening as observed for the adjacent residues 165, 171, and 172.

Order parameters (S^2) and rotational correlation time (τ_c)

τ_c. An effective rotational correlation time ($\tau_{c,i}$) at each residue has been calculated from J(0) and J(ω_N) spectral densities using Eq. (1).[36,37] PrP(113–231) exhibits a good deal of variation in the rotational correlation time $\tau_{c,i}$ per residue, shown as Supporting Figure S3. This reflects both fast internal motions and slow segmental rearrangements in addition to the over-all rotational diffusion time. A trimmed mean rotational correlation time has been determined in order that only rigid amide nitrogens are used in the calculation of τ_c.[38] This has been achieved by using only residues that have heteronuclear NOEs greater than 0.72, so as to eliminate fast pico-second motions. Furthermore, the residues with unusually high R_2 rates, reflecting slow R_{ex} motions, have also been eliminated from the calculation of rotational correlation time. This trimmed rotational correlation time produces a mean value of 9.0 ns for residues within the three helices. There is still some variation in the rotational correlation time, residues in helix A give consistently lower τ_c values with a mean of 8.1 ± 0.2 ns, residues in helix B have a mean τ_c value of 8.4 ± 0.6 ns, whereas helix C gives consistently higher values with a mean of 9.9 ± 0.4 ns as is apparent from the Supporting Figure S3. If the protein does not approximate to a sphere, then individual τ_c values will vary according to the angle between the NH bond vector and the long axis of the protein.[39] The differences in τ_c from the three helices reflect anisotropic tumbling within the molecule. The variation in τ_c between helices have been shown to correlate well with asymmetric hydrodynamic radius calculated for PrP^C with the long axis, R_z of 24 Å and 16 and 12 Å for the shorter axis, R_x and R_y.[15] It has previously been shown from calculations using the PrP^C solution structures show that the N—H bond vectors of helix C are parallel to the long axis, whereas helix A is perpendicular to it.[15]

S^2. The model-free formalism[40,41] is often used to describe the motions of a protein. In particular, the order parameter (S^2) describes the amplitude of the nanosecond time-scale motions and can range between 0 and 1.0, representing complete disorder and complete order, respectively. Approximate order parameters have been directly calculated from J(0) and J(ω_N) spectral densities using Eq. (2)[36,37] rather than a statistical selection of various models of motion.[42] The correlation time τ_c for the protein has been allowed to vary on a per-residue-basis. The order parameters for mPrP(112–231) are shown in Figure 5(a), and the S^2 values have been mapped on to the structure of $mPrP^C$, Figure 5(b). Apart from the four residues identified as containing R_{ex} motions, all residues produce order parameters less than 1.0. The three helical regions give very similar order parameters, typical for a well ordered protein, with very similar mean S^2 values of 0.91, 0.92, and 0.92 for helices A, B, and C, respectively. Residues between the first β-strand and helix A exhibit very slightly increased flexibility (in particular I138) with S^2 values of ~0.8. Considerable flexibility, with $S^2 < 0.75$, are observed for residues between 113 and 125 at the N-terminus, the loop region between helix B and C (residues N196 and F197) and residue R229 at the C-terminus of PrP^C.

Discussion

Order parameters calculated for truncated PrP^C

^{15}N relaxation measurements have previously been reported for full-length PrP(29–231)[15] and the 90–231 fragment.[15,31] The full-length protein and truncated fragments contain a significant amount of the unstructured tail, residues 23–125. This long-tail attached to the C-terminal globular domain of PrP^C appears to have a profound influence of the relaxation behavior of the structured C-terminus. In particular, attempts to obtain an order parameter (S^2) for each NH bond vector have been unsuccessful for the majority of residues in helix B and C, for both PrP(29–231) and the shorter fragment PrP(90–231),[15] with S^2 driven to values considerably higher than the physical limit of 1.0. One explanation is that the long unstructured tail causes disproportionately short T_2 values relative to T_1 and heteronuclear NOEs making the determination of an order parameter intractable. This was somewhat of a surprise as other unstructured proteins have been readily fitted to model free formalism by using a variable rotational correlation time calculated per-residue.[43] Furthermore, the removal of a significant proportion of the unstructured tail of PrP^C residues 29–90, had no effect on the dynamics of the protein as ^{15}N relaxation parameters for SHaPrP(90–231) and SHaPrP(29–231) are strikingly similar.[15] Alternatively, we postulated that much of the structured domain might exhibit pronounced additional slow segmental exchange motions, and these would cause

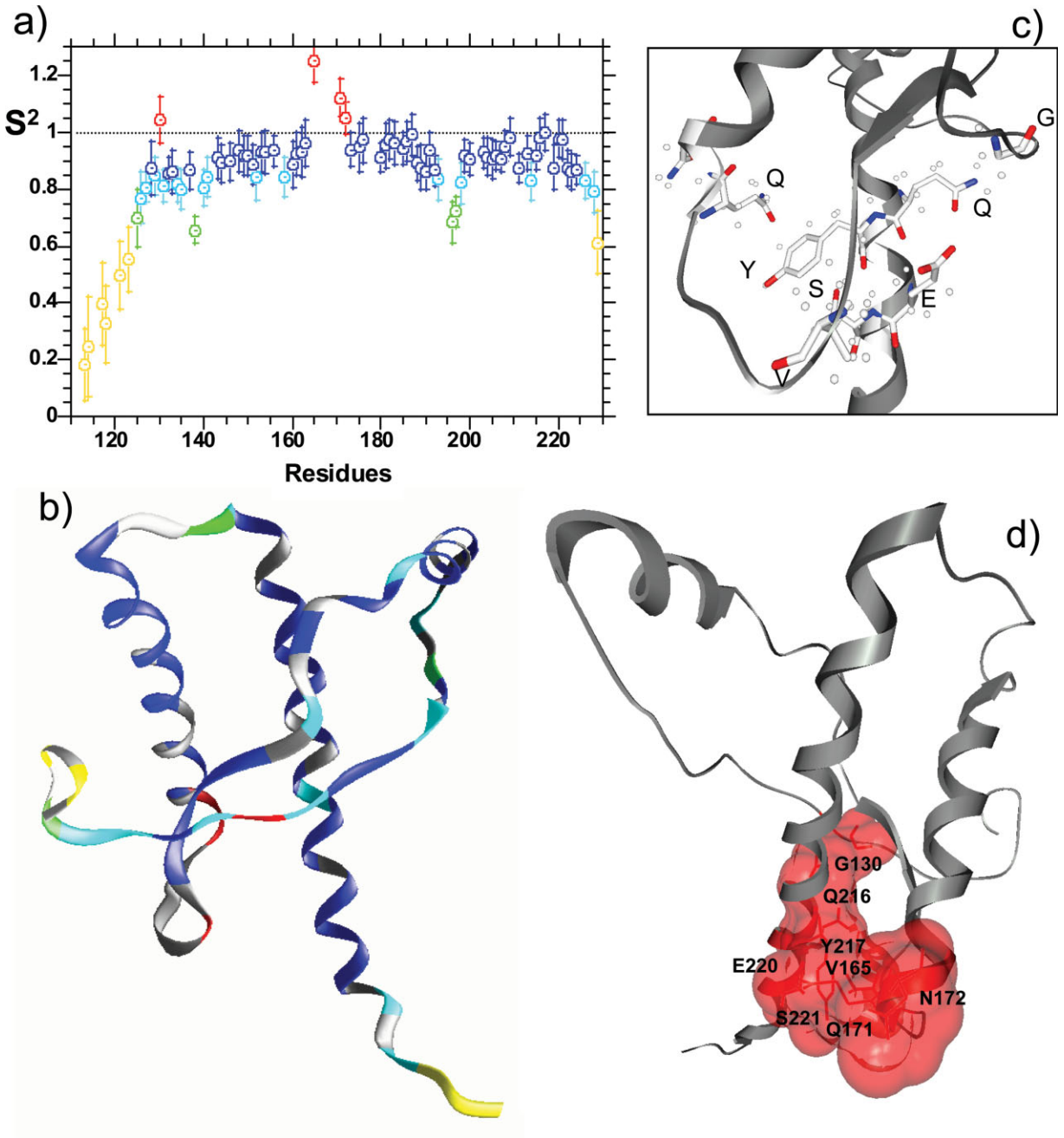

Figure 5. **(a)** Order parameters (S^2) for mPrP(113–231). Order parameters describe the amplitude range of the nanosecond time-scale motions between 0 (flexible) and 1.0 (rigid). Residues that exhibit additional R_{ex} exchange motions are highlighted in red. **(b)** Order parameter mapped onto the structure (1 xyx) of PrP^C: red $S^2 > 1.0$ (R_{ex} motions); blue $0.85 < S^2 < 1.0$; cyan $0.75 < S^2 < 0.85$; green $0.65 < S^2 < 0.75$; and yellow $S^2 < 0.65$, residues in gray have no value calculated. **(c)** Slow conformational fluctuations are localized to a distinct region within PrP^C, the position of side-chains that exhibit R_{ex} motions are highlighted, dots are proton positions. **(d)** The molecular surface, in red, generated by the residues that exhibit R_{ex} motions, within the context of the whole structured domain. This figure was generated using GRASP2.

disproportionately short T_2 times. A large number of residues exhibiting significant exchange motions on a milli-second to micro-second time scale was a particularly appealing hypotheses to explain the unusually long transverse relaxation rates, bearing in mind the ability of PrP^C to misfold into a pathogenic isoform. With this in mind, we set about determining the ^{15}N relaxation behavior of the truncated fragment of PrP^C containing only the structured domain residues 113–231, so eliminating the effect of the unstructured tail. Comparison of mPrP(113–231) with relaxation data for the longer fragment and full-length PrP highlights the influence of the long unstructured tail on the hydrodynamics of the whole protein. Relaxation data published

for full-length Syrian-hamster PrP, and the 90–231 fragments were recorded at the same temperature and pH as this study[15] and therefore permits direct comparison.

The magnitude and trend of R_1 rates and heteronuclear NOEs are strikingly similar for all three fragments; SHaPrP(29–231), SHaPrP(90–231),[15] and mPrP(113–231). In particular, R_1 values for the bulk of residues are largely invariant and produce R_1 rates of $\sim$1.5 s^{-1} for all three constructs. Similarly, heteronuclear-NOE values for residues within the helices of PrP^C exhibit very similar values for all three constructs – typically 0.80. In contrast, R_2 values for the short fragment that lacks the unstructured N-terminal tail exhibits strikingly different R_2 rates. The structured domain, particularly the three helices, give R_2 values between 16 and 20 s^{-1} for both SHaPrP(90–231) and SHaPrP(29–231), whilst for PrP(113–231), R_2 rates are significantly reduced with average values between 11.2 s^{-1} (helix A) and 13.5 s^{-1} (helix C). The reduction in the R_2 rates between PrP(90–231) and PrP(113–231) can not simply be accounted for by the very small reduction in molecular weight that is the loss of 14 amino acids (from 141 amino acids to 118 + 9, for the His-tag). It is clear that the presence of a flexible tail causes the disproportionably large R_2 rates relative to R_1 and heteronuclear NOEs making the determination of an order parameter intractable. Removal of the flexible tail significantly reduces R_2 rates while leaving R_1 and heteronuclear NOEs largely unaffected. This means the R_2 values reflect the hydrodynamics of a globular protein and order parameters can readily be calculated.

It is clear from this study that even when the rotation correlation time is permitted to vary, per-residue, the calculation of an order parameter may not be appropriate for proteins with appreciable portions of unfolded polypeptide chain. Thus each N—H vector is better described by a distribution of rotational correlation times.[44] Our study suggests that large portions of PrP^C do not exhibit slow R_{ex} motions, as simply removing the flexible tail causes a dramatic reduction in R_2 values. The effect on the R_2 rates is sufficiently significant to facilitate, for the first time, the determination of order parameter (S^2), for the PrP(113–231) fragment. It is notable that order parameters (S^2) calculated do not require a term for R_{ex} motions and yet the S^2 values are typical for a globular protein for the overwhelming majority of residues. In contrast, the majority of residues for full-length PrP have S^2 values in excess of 1.0.

J(0) and S^2 can reflect internal flexibility of the NH bond vector, in particular, a value for J(0) less than $2/5\tau_m$ indicates internal flexibility of the NH bond.[29] However, J(0) is strongly influenced by the rotational correlation time of the protein, and for this reason anisotropic tumbling can influence J(0) spectral densities. This is the case for PrP^C, where it has been shown that the structured domain is not isotropic with a the long axis, R_z of 24 Å and two shorter axis, R_x; 16 and R_y; 12 Å.[15] It has been shown that helix C, the longer of the three helices, is aligned with long axis while helix A is perpendicular to it. This anisotropic tumbling results in mean J(0) values for helix C larger than helix A; 3.6 ns relative to 3.0 ns for mPrP(113–231). Calculations using the PrP^C solution structures show that the N—H bond vectors of helix C are parallel to the long axis while helix A is perpendicular to it. In contrast, S^2 order parameters indicate H—N bond motional amplitude distinct from a rotational correlation time. The value set for the rotational correlation time will clearly influence the order parameter.[45] However, here we allow τ_c to vary per residue, which therefore compensates for the effect of an anisotropic rotational diffusion within PrP^C, as shown in Supporting Figure S3. Inspection of the S^2 data [Fig. 5(b)] shows that all three helices have very similar mean S^2 values 0.91, 0.92, and 0.92 for helices A, B, and C, respectively. It is clear that an asymmetric rotational diffusion is reflected in J(0) values, but the values of the order parameters, calculated with a variable τ_{ci} are not influenced by asymmetric rotational diffusion.

The similarities between structures of mammalian PrP species are well documented.[8] Sequence comparison of mouse and Syrian hamster shows a 94.2% homology in this fragment, there are six largely conservative substitutions. It is clear from this study that mouse and hamster PrP have very similar dynamical properties. Comparison of $J(0.87\omega_H)$ spectral densities between mouse and hamster show very similar trends. In particular, the flexible N-terminal tail stretches between residues 23 and 125, whereas the flexibility at the C-termini is limited to the last few residues. In addition, both proteins have a flexible loop between helix B and C, residues 190–197, which possesses fast pico-second time-scale motions.

PrP^C folding intermediates and stability

PrP*, the precursor for amyloid formation, could require the complete unfolding of PrP^C. Alternatively, PrP^C could be a kinetically trapped intermediate to the formation of PrP* and PrP^{Sc}. Finally, PrP* might represent a sampled conformation formed on the way to a more stable native PrP^C, as described in Supporting Figure S4. It is yet to be established whether PrP^{Sc} retains any of the structural elements found in PrP^C, although recent data suggests that residues 160–220 undergo significant conformation change to form amyloid fibers.[13,24] In contrast, modeling based on 2D crystals,[46] and epitope mapping studies[47] of PrP^C and PrP^{Sc}, as well as the presence of the intra-molecular disulphide in PrP^{Sc},[48] suggests that much of helix B and C may be retained in the scrapie form. At face value, the J(0) values hint at the possibility that helix A of PrP^C has relatively more flexibility than helix B

and C. However, the effect of anisotropic tumbling needs to be taken into account. This has been achieved by determining the order parameters, which give very similar S^2 values for all three helices. Hence, helix A does not have any more internal flexibility than the other helices. This observation agrees with measurements of PrP^C amide protection factors.[49] This study indicated that all three helices have similar hydrogen-bond protection factors, apart from a few amides adjacent to the single disulphide bond within PrP, Cys190–Cys214, which exhibit additional amide protection.[50] These observation support reports that, at neutral pH, PrP^C undergoes essentially a simple two state unfolding, from native to fully unfolded.[51,52] An intermediate in which, for example, helix A is unfolded and helix B and C remain intact is not suggested.

Studies using hydrostatic pressure[53] have been used to study the unfolding of PrP^C in an attempt to identify folding intermediates. These folding intermediates may represent conformations of the prion protein (PrP*) on a pathway to PrP^{Sc} and amyloid formation. Perhaps contradictory to the modeling based on 2D crystals,[46] these studies suggest that a largely intact helix B and C is unlikely. Indeed, the NMR studies suggest that helix A actually has slightly more stability than helix B or C.[32,53] Recent amide protection studies of prion fibrils (PrP^{Sc} rather than PrP^C) have indicated that a relatively short stretch of the sequence constitutes the β-sheet rich core of PrP^{Sc} between residues 169 and 214,[24] again supporting the assertion that helix B and C are not retained as helices in the PrP* precursor to the scrapie isoform.

Mutations in the prion protein linked with familial prion disease are found throughout the PrP sequence, some of these residues, in particular D178N, T183A, and Q217R involve disruption of salt-bridges or hydrogen-bond net works and seem to destabilize the native structure.[7] Other mutations are found in the unstructured region of PrP^C, residues; 102, 105, 117 for example. These mutations may stabilize the formation of PrP* and PrP^{Sc} rather than destabilize PrP^C. Furthermore, it has been shown that residues 90–126, although unstructured in PrP^C, are essential for prion propagation. Removal of these residues (as with the construct studied here) does not destabilize PrP^C supporting the hypotheses that these residues stabilize the formation of PrP*. It is interesting to note that a genetic mutation, which has a stop codon at residue 145, generates a truncated PrP fragment residues 23–145. This fragment lacks residues from helix B and C, but still causes a familial prion disease.[54]

Slow conformational fluctuations are localized to a distinct region within PrP^C

Slow motions that cause exchange broadening of NMR signals are typically because of large segmental motions rather than single hydrogen-bond rearrangements. Residues exhibiting exchange broadening sample alternative conformations in exchange with the native conformation on a milli-micro second timescale. Exchange motions in the short anti-parallel β-sheet, in particular at reside G130, are interesting as polymorphism in human PrP is found at the adjacent residue 129M/L. This polymorphism dictates strain-type in familial prion disease and is a key determinant of susceptibility to sporadic and acquired CJD. In particular, only individuals homozygous for methionine at 129 (Met/Met) (with one exception) have contracted variant CJD.[55] Slow exchange motions observed for mPrP at G130 are also observed for Syrian hamster PrP at the same position and at the adjacent β-sheet V161.

Residues 165, 171, and 172 also show large R_{ex} motions while residues in the loop between them (166–170, between the β-strand S2 and the start of helix B) give weak NMR signals, which may be a result of broadening because of R_{ex} motions. NMR studies on a number of different mammalian prion proteins have exhibited similar weak signals in this loop.[11] Although for hamster PrP residues between 165 and 172 do not seem to show marked exchange broadening.[15] The N170S mutation, hamster to mouse, seems to explain the differences in flexibility for residues 165, 171, and 172.

Residues Q216, Y217, E220, and S221 in mouse PrP show large J(0) spectral densities (greater than 4 ns, >2 standard deviations from the mean J(0) for helix C) indicating that these residues may also exhibit some R_{ex} motions. The analogous residues for hamster PrP are not identified as having pronounced J(0) values although the noise in these larger fragments is considerably increased and could well account for them going undetected.

Inspection of the $mPrP^C$ solution structure (1 xyx)[4,7] indicates that the residues exhibiting some slow exchange line broadening, 216, 217, 220, and 221, lie along the same face of helix C and interact with residues exhibiting significant R_{ex} motion in the loop between V165 and N172. Figure 5(c) shows that G130 is close to Q216, whilst tyrosine Y217 sits in behind the 165–172 loop and forms hydrophobic packing interactions with V165 and Q171, S221 is also spatially close to V165. Thus, rather than simply the β-sheet exhibiting slow conformational fluctuations in PrP^C, the residues exhibiting R_{ex} motions can all be mapped to a localized patch or inter-linked region, as indicated in Figure 5(d). As we have been unable to define the R_{ex} motion of residues 166–170, they don't appear in Figure 5(d), but would extend the localized patch of residues involved in slow conformational fluctuations. Intriguingly, residues Q167, Q171, V214, and Q218 have been identified as the binding site for the so-called "protein X".[56] These residues exhibit, or are sequentially adjacent to residues that exhibit, R_{ex} motions. The binding of an as yet, unidentified molecule might destabilize PrP^C or stabilize a PrP*

intermediate. Furthermore, a mutation in humans that causes familial prion disease, Q217R (Q216 in mouse), has been identified and is likely to destabilize this region.[7]

Interestingly, Doppel protein which has both sequence and structural homology with PrP^{57} is less stable than PrP^{C}[50] but will not propagate prions. One key difference with Doppel is the presence of a second disulphide. This disulphide is found between the loop region and helix C (equivalent residues in the mouse sequence are residues 166 and 221).[58] This is the same region that exhibits slow conformational fluctuations in PrP^{C}. Perhaps, a key difference with Doppel is the stabilization of this region of the protein via an additional disulphide bond.

Profiling methods for determining fibril-forming segments of proteins have identified residues 170–175 (SNQNNF) within mouse and human PrP.[59] This hexapeptide will form fibrils and the closely related microcrystals. It is suggested that the fundamental unit of amyloids is the tightly interdigitated β-sheets, termed steric zippers, formed by the cross-β stacking of these residues.[59] This sequence with its high complimentary interface might nucleate fibrilization. It is notable that residues N171 and Q172 on the surface of $mPrP^{C}$ exhibit slow motion conformational fluctuations. It is a possibility that the flexibility within these residues could facilitate the recognition process as PrP^{C} docks on to the exposed ends of amyloid fibers during fiber elongation. The region identified here as possessing conformational fluctuations might represent a possible therapeutic target, inhibiting the PrP^{C}–PrP^{Sc} recognition process or stabilizing PrP^{C}.

Materials and Methods

Expression and purification of recombinant mPrP(113–231)

C-terminally His-tagged full-length mouse PrP(23–231) was cloned into a pET-23 vector as previously described.[60] Codons for amino acid residues 23–112 were deleted by mutation of the sequence to include and NdeI site prior to the codon for residue 113. After restriction digestion with NdeI (Promega), the plasmid was religated and expressed a truncated PrP fragment, PrP(113–231) which lacks the natively unstructured N-terminal domain. This fragment retains a methionine residue prior to residue 113. The protein was expressed in 2-L flasks of Escherichia coli BL21(DE3) cells in ^{15}N labeled minimal medium containing (1 g/L) $^{15}NH_4Cl$ (Cambridge isotope laboratories) as the sole nitrogen source. Cultures were grown at 37°C to an A_{600} of 0.9 and the protein expression was induced by the addition of isopropyl-β-D-thiogalactopyranoside to a final concentration of 1 m*M*. Bacterial pellets were harvested after 4 h and sonicated in a resuspension buffer containing 8*M* urea, 200 m*M* NaCl, and 50 m*M* Tris, pH 7.6. The resulting solution was cleared of bacterial debris by centrifugation at 6000*g* for 15 min. The protein was absorbed to a nickel-charged metal affinity column made from chelating Sepharose (Amersham Biosciences). The proteins were washed with at least 20 column volumes of resuspension buffer and eluted from the column using the same buffer supplemented with 300 m*M* imidazole. The protein was found to be greater than 95% pure by polyacrylamide electrophoresis and Coomassie staining. The protein was refolded by successive rounds of dilution in deionized water and concentrated in a Vivaspin centrifugal concentrator (Vivascience) with a 10,000 molecular weight cut off. The refolded protein was dialyzed twice at 4°C against deionized water to remove residual urea. The concentration of mPrP(113–231) was measured by its absorbance at 280 nm and confirmed by Bicinchoninic Acid (BCA) assay (Sigma).

Preparation of NMR sample. NMR samples contained; 0.6 mL of 3.15 mg/mL His tagged ^{15}N mouse PrP(113–231) in 20 m*M* sodium acetate and 10% D_2O at pH 5.32.

NMR resonance assignments

All NMR spectra were acquired at 30°C on a 600 MHz Bruker Avance spectrometer equipped with a 5 mm inverse detection triple-resonance *z*-gradient probe. Phase-sensitive 2D ^{15}N-HSQC spectra were acquired using Echo-antiecho gradient selection. ^{1}H acquisition parameters were 0.122 sec acquisition time, 1 sec fixed delay and 2048 complex (t_2) points, whereas 256 complex points were collected for the ^{15}N dimension. Thirty-two transients were recorded for each t_1 interval. The ^{1}H and ^{15}N dimensions possessed spectral widths of 14 ppm and 32 ppm, respectively. The ^{15}N dimension was zero filled to 256 data points before squared-cosine apodization and Fourier transformation. Three-dimensional phase sensitive ^{15}N-HSQC-NOESY[61] and ^{15}N-HSQC-TOCSY spectra[62] were acquired using Echo-antiecho gradient selection. The 3D ^{15}N-HSQC-TOCSY and 3D ^{15}N-HSQC-NOESY spectra were obtained using a mixing time of 60 ms and 150 ms, respectively. For both experiments, 2048 complex points were collected in the direct ^{1}H dimension over a spectral width of 12 ppm, whereas 64 complex points and 160 complex points were collected for the indirect ^{15}N and ^{1}H dimensions respectively over a ^{15}N spectral width of 32.2 ppm and a ^{1}H spectral width of 12 ppm. Both spectra were zero filled to 2048 data points in the direct ^{1}H dimension, 128 data points in the indirect ^{15}N dimension and 512 data points in the indirect ^{1}H dimension. All NMR data was processed in XWINNMR (Bruker) and analyzed in XEASY.[63] Resonance assignments were made manually using sequential ^{1}H NOE connectivities with comparison to assignments deposited in the Biological Magnetic Resonance Databank (www.bmrb.wisc.edu) for related

mammalian prion proteins, in particular human and Syrian hamster PrP.

^{15}N NMR relaxation measurements

All relaxation measurements were performed at a temperature of 30°C. The pulse sequences used to obtain T_1, T_2, and heteronuclear NOE spectra are those described by Farrow *et al.*,[64] which employ gradient selection and sensitivity enhancement, as well as minimal water suppression.

Three pairs of saturated and non-saturated[20]-^{15}N heteronuclear NOE experiments were recorded at 600 MHz (60.8 MHz ^{15}N frequency). In the direct (^{1}H) dimension, the carrier frequency was set on the water resonance with a spectral width of 14 ppm; the indirect (^{15}N) dimension was centered at 118 ppm with a 30 ppm spectral width. 2K complex data points with 128 complex increments were collected. Each of the-^{15}N NOE experiments was acquired with 80 scans.[20] The ^{1}H saturation was achieved by the application of 120° ^{1}H pulses separated by 18 ms, for a 3 s period. In addition, a 4 sec recycle delay was used.

Twelve time points were collected for both T_1 and T_2 experiments, and each set included duplicate measurements to allow estimation of the uncertainty. The delays used were as follows:

T_1 Delays = 2, 2, 64, 128, 256, 384, 512, 768, 768, 1024, 1024, 1536 ms

T_2 Delays = 16, 16, 32, 48, 64, 96, 96, 128, 128, 192, 192, 256 ms

Repeated numbers indicate duplicate measurements. ^{15}N T_1 and T_2 relaxation times were obtained from running phase-sensitive 2D ^{15}N-HSQC spectra acquired with Echo/antiecho gradient selection as described above. Typical T_1 experiments were acquired with 16 scans and a repetition delay of 3 sec, whereas T_2 experiments were acquired with 16 scans and a 500 μs delay between 180 pulses in the Carr–Purcell–Meiboom–Gill (CPMG) pulse train and a 3 sec repetition delay.

NMR relaxation data processing

All spectra were processed using the Bruker NMR software. Spectra were zero filled to 4 K by 1 K points in the t_2 and t_1 dimensions respectively and were apodized using a phase-shifted sinebell squared function. Residual water signal was removed using a low frequency filter. Cross-peak intensity was measured as peak height rather than volume, to reduce errors associated with peak over-lap. Fourier transformed data was exported into the Tripos Sybyl 7.0 NMR TRIAD programmed. The peak height intensity was obtained by curve fitting to polynomial function for each peak. This is a preferred method rather than a searching for peak maximal which can introduce a systematic bias.[65] Weak intensity peaks, at the longer relaxation delay times are particularly prone to systematic bias when a search routine to pick peak maxima is used.[65]

The heteronuclear NOE values were obtained from the ratio of peak intensity for ^{1}H-saturated and unsaturated spectra. The mean and standard deviation for the heteronuclear-NOE data was calculated from three pairs of experiments. To obtain mono-exponential decay curves for T_1 and T_2 relaxation data peak intensities (by height) were fitted to a two-parameter equation: $I(t) = I_0 e^{-t/T_n}$, where I = intensity, t = delay in CPMG or longitudinal delay, $T_n = T_1$ or T_2 value.[66] This data was compared to relaxation values using a three parameter equation; $I(t) = I_\infty + I_0 e^{-t/Tn}$, where I_∞ is the offset intensity from zero at infinite time. Comparison of relaxation values obtained using a two or three parameter fits confirmed that possible systematic errors and bias in the data had not been introduced by using a two-parameter fit.[65] The standard error for the R_1 and R_2 values was determined directly from the curve fit routine.

Spectral density functions and order parameters

Reduced spectral densities map the motion of each NH bond at frequencies $\omega = 0$, ω_N, and $0.87\omega_H$.[34,35] Reduced spectral density assumes a single spectral density for $J(\omega_H + \omega_N)$, $J(\omega_H)$, and $J(\omega_H - \omega_N)$ of $J(0.87\omega_H)$. The spectral densities at these three frequencies were obtained using an in-house script; DUGGAN, from the relaxation rates R_1 ($1/T_1$), R_2 ($1/T_2$) and the hetero-nuclear NOE using four equations described by Farrow *et al.*[34,67] and shown as Supporting Information. The constant for chemical shift anisotropy was set at −170 ppm and the NH bond length was set to 1.02 Å.[39]

The model-free formalism[40,41] can be used to describe the motions of a protein in terms of a rotational correlation time (τ_c) and an order parameter (S^2). The most widely used model-free formalism assumes isotropic tumbling.[40,41] In this case, τ_c is identical for each amide. The approach selects various descriptors of the motion using statistical criteria as described by Mandel *et al.*[42] We have chosen not to use this approach, instead here we have calculated an effective rotational correlation time ($\tau_{c,i}$) at each residue directly from $J(0)$ and $J(\omega_N)$ spectral densities according to Eq. (1).[36,37]

$$\tau_{c,i} = 1/\omega_N\{(J(0)_i - J(\omega_N)_i)/J(\omega_N)_i\}^{1/2} \qquad (1)$$

Furthermore, an approximate order parameter (S^2) has been obtained directly from $J(0)$ and $J(\omega_N)$ using Eq. (2).[36,37]

$$S^2 = 5/2\ \{J(0) - J(\omega_N)\}(1 + \omega_N^2\tau_c^2)/(\omega_N^2\tau_c^3) \qquad (2)$$

This approximation of S^2 does not require the statistical selection of various descriptions of the motion[42,68] as the calculation of the order parameter

does not incorporate additional fast internal motions on the pico-second time scale (τ_e) or slower segmental motions on the milli- to micro-second time-scale (R_{ex}). Furthermore, the rotation correlation time is permitted to vary, per-residue, removing the possible effects of an anisotropic rotational diffusion tensor. Although an approximation of the order parameter, the values represent a reasonable description of the amplitude of the nanosecond time scale motions, as the order parameter values (S^2) are largely insensitive to the presence or absence of a descriptor for fast pico-second time scale (τ_e) motions. In addition, any residues that contains significant milli- to micro-second time-scale (R_{ex}) motions can be identified from J(0) spectral densities.

Acknowledgments

C.E.J. acknowledges the support of the University of Queensland Postdoctoral Fellowship. The authors are grateful to Brendan Duggan for providing his script to calculate spectral densities. Also thanks to Grainne for the birth of Abbie Caoirmhe Viles, on March 27, 2008.

References

1. Prusiner SB (1998) Prions. Proc Natl Acad Sci USA 95: 13363–13383.
2. Legname G, Baskakov IV, Nguyen HO, Riesner D, Cohen FE, DeArmond SJ, Prusiner SB (2004) Synthetic mammalian prions. Science 305:673–676.
3. Silveira JR, Raymond GJ, Hughson AG, Race RE, Sim VL, Hayes SF, Caughey B (2005) The most infectious prion protein particles. Nature 437:257–261.
4. Riek R, Hornemann S, Wider G, Billeter M, Glockshuber R, Wuthrich K (1996) NMR structure of the mouse prion protein domain PrP(121–321). Nature 382:180–182.
5. Donne DG, Viles JH, Groth D, Mehlhorn I, James TL, Cohen FE, Prusiner SB, Wright PE, Dyson HJ (1997) Structure of the recombinant full-length hamster prion protein PrP(29–231): the N terminus is highly flexible. Proc Natl Acad Sci USA 94:13452–13457.
6. James TL, Liu H, Ulyanov NB, Farr-Jones S, Zhang H, Donne DO, Kaneko K, Groth D, Mehlhorn I, Prusiner SB, Cohen FE (1997) Solution structure of a 142-residue recombinant prion protein corresponding to the infectious fragment of the scrapie isoform. Proc. Natl. Acad. Sci. USA 94: 10086–10091.
7. Riek R, Wider G, Billeter M, Hornemann S, Glockshuber R, Wuthrich K (1998) Prion protein NMR structure and familial human spongiform encephalopathies. Proc Natl Acad Sci USA 95:11667–11672.
8. Zahn R, Liu A, Luhrs T, Riek R, von Schroetter C, Lopez Garcia F, Billeter M, Calzolai L, Wider G, Wuthrich K (2000) NMR solution structure of the human prion protein. Proc Natl Acad Sci USA 97:145–150.
9. Lopez Garcia F, Zahn R, Riek R, Wuthrich K (2000) NMR structure of the bovine prion protein. Proc Natl Acad Sci USA 97:8334–8339.
10. Calzolai L, Lysek DA, Perez DR, Guntert P, Wuthrich K (2005) Prion protein NMR structures of chickens, turtles, and frogs. Proc Natl Acad Sci USA 102:651–655.
11. Gossert AD, Bonjour S, Lysek DA, Fiorito F, Wuthrich K (2005) Prion protein NMR structures of elk and of mouse/elk hybrids. Proc Natl Acad Sci USA 102:646–650.
12. Lysek DA, Schorn C, Nivon LG, Esteve-Moya V, Christen B, Calzolai L, von Schroetter C, Fiorito F, Herrmann T, Guntert P, Wuthrich K (2005) Prion protein NMR structures of cats, dogs, pigs, and sheep. Proc Natl Acad Sci USA 102:640–645.
13. Cobb NJ, Sonnichsen FD, McHaourab H, Surewicz WK (2007) Molecular architecture of human prion protein amyloid: a parallel, in-register β-structure. Proc Natl Acad Sci USA 104:18946–18951.
14. Lu X, Wintrode PL, Surewicz WK (2007) β-sheet core of human prion protein amyloid fibrils as determined by hydrogen/deuterium exchange. Proc Natl Acad Sci USA 104:1510–1515.
15. Viles JH, Donne D, Kroon G, Prusiner SB, Cohen FE, Dyson HJ, Wright PE (2001a) Local structural plasticity of the prion protein. Analysis of NMR relaxation dynamics. Biochemistry 40:2743–2753.
16. Brown DR, Qin K, Herms JW, Madlung A, Manson J, Strome R, Fraser PE, Kruck T, von Bohlen A, Schulz-Schaeffer W, Giese A, Westaway D, Kretzschmar H (1997) The cellular prion protein binds copper in vivo. Nature 390:684–687.
17. Viles JH, Cohen FE, Prusiner SB, Goodin DB, Wright PE, Dyson HJ (1999) Copper binding to the prion protein: structural implications of four identical cooperative binding sites. Proc Natl Acad Sci USA 96:2042–2047.
18. Garnett AP, Viles JH (2003) Copper binding to the octarepeats of the prion protein. Affinity, specificity, folding, and cooperativity: insights from circular dichroism. J Biol Chem 278:6795–6802.
19. Jones CE, Abdelraheim SR, Brown DR, Viles JH (2004) Preferential Cu^{2+} coordination by His96 and His111 Induces {β}-sheet formation in the unstructured amyloidogenic region of the prion protein. J Biol Chem 279: 32018–32027.
20. Jones CE, Klewpatinond M, Abdelraheim SR, Brown DR, Viles JH (2005) Probing $copper^{2+}$ binding to the prion protein using diamagnetic $nickel^{2+}$ and ^1H NMR: the unstructured N terminus facilitates the coordination of six $copper^{2+}$ ions at physiological concentrations. J Mol Biol 346:1393–1407.
21. Klewpatinond M, Davies P, Bowen S, Brown DR, Viles JH (2008) Deconvoluting the Cu^{2+} binding modes of full-length prion protein. J Biol Chem 283:1870–1881.
22. Zahn R (2003) The octapeptide repeats in mammalian prion protein constitute a pH-dependent folding and aggregation site. J Mol Biol 334:477–488.
23. Baskakov IV, Legname G, Baldwin MA, Prusiner SB, Cohen FE (2002) Pathway complexity of prion protein assembly into amyloid. J Biol Chem 277:21140–21148.
24. Swietnicki W, Morillas M, Chen SG, Gambetti P, Surewicz WK (2000) Aggregation and fibrillization of the recombinant human prion protein huPrP90-231. Biochemistry 39:424–431.
25. Baskakov IV, Legname G, Prusiner SB, Cohen FE (2001) Folding of prion protein to its native α-helical conformation is under kinetic control. J Biol Chem 276: 19687–19690.
26. Morillas M, Vanik DL, Surewicz WK (2001) On the mechanism of α-helix to β-sheet transition in the recombinant prion protein. Biochemistry 40:6982–6987.
27. Gerber R, Tahiri-Alaoui A, Hore PJ, James W (2007) Oligomerization of the human prion protein proceeds via a molten globule intermediate. J Biol Chem 282: 6300–6307.
28. O'Sullivan DB, Jones CE, Abdelraheim SR, Thompsett AR, Brazier MW, Toms H, Brown DR, Viles JH (2007) NMR characterization of the pH 4 β-intermediate of the prion protein: the N-terminal half of the protein remains

unstructured and retains a high degree of flexibility. Biochem J 401:533–540.
29. Dayie KT, Wagner G, Lefevre JF (1996) Theory and practice of nuclear spin relaxation in proteins. Annu Rev Phys Chem 47:243–282.
30. Palmer AG III (1997) Probing molecular motion by NMR. Curr Opin Struct Biol 7:732–737.
31. Liu H, Farr-Jones S, Ulyanov NB, Llinas M, Marqusee S, Groth D, Cohen FE, Prusiner SB, James TL (1999) Solution structure of Syrian hamster prion protein rPrP(90–231). Biochemistry 38:5362–5377.
32. Kuwata K, Kamatari YO, Akasaka K, James TL (2004) Slow conformational dynamics in the hamster prion protein. Biochemistry 43:4439–4446.
33. Daniels M, Cereghetti GM, Brown DR (2001) Toxicity of novel C-terminal prion protein fragments and peptides harbouring disease-related C-terminal mutations. Eur J Biochem 268:6155–6164.
34. Farrow NA, Zhang O, Forman-Kay JD, Kay LE (1995a) Comparison of the backbone dynamics of a folded and an unfolded SH3 domain existing in equilibrium in aqueous buffer. Biochemistry 34:868–878.
35. Peng JW, Wagner G (1995) Frequency spectrum of NH bonds in eglin c from spectral density mapping at multiple fields. Biochemistry 34:16733–16752.
36. Lefevre JF, Dayie KT, Peng JW, Wagner G (1996) Internal mobility in the partially folded DNA binding and dimerization domains of GAL4: NMR analysis of the N-H spectral density functions. Biochemistry 35:2674–2686.
37. Bracken C, Carr PA, Cavanagh J, Palmer AG IIIrd (1999) Temperature dependence of intramolecular dynamics of the basic leucine zipper of GCN4: implications for the entropy of association with DNA. J Mol Biol 285: 2133–2146.
38. Barbato G, Ikura M, Kay LE, Pastor RW, Bax A (1992) Backbone dynamics of calmodulin studied by 15N relaxation using inverse detected two-dimensional NMR spectroscopy: the central helix is flexible. Biochemistry 31: 5269–5278.
39. Tjandra N, Wingfield P, Stahl S, Bax A (1996) Anisotropic rotational diffusion of perdeuterated HIV protease from 15N NMR relaxation measurements at two magnetic fields. J Biomol NMR 8:273–284.
40. Lipari G, Szabo A (1982) Model-free approach to the interpretation of nuclear magnetic resonance relaxation in macromolecules. 2. Analysis of experimental results. J Am Chem Soc 104:4559–4570.
41. Lipari G, Szabo A (1982) Model-free approach to the interpretation of nuclear magnetic resonance relaxation in macromolecules. 1. Theory and range of validity. J Am Chem Soc 104:4546–4559.
42. Mandel AM, Akke M, Palmer AG IIIrd (1995) Backbone dynamics of Escherichia coli ribonuclease HI: correlations with structure and function in an active enzyme. J Mol Biol 246:144–163.
43. Farrow NA, Zhang O, Forman-Kay JD, Kay LE (1997) Characterization of the backbone dynamics of folded and denatured states of an SH3 domain. Biochemistry 36: 2390–2402.
44. Buevich AV, Baum J (1999) Dynamics of unfolded proteins: Incorporation of distributions of correlation times in the model free analysis of NMR relaxation data. J Am Chem Soc 121:8671–8672.
45. Osborne MJ, Wright PE (2001) Anisotropic rotational diffusion in model-free analysis for a ternary DHFR complex. J Biomol NMR 19:209–230.
46. Govaerts C, Wille H, Prusiner SB, Cohen FE (2004) Evidence for assembly of prions with left-handed β-helices into trimers. Proc Natl Acad Sci USA 101: 8342–8347.
47. Peretz D, Williamson RA, Matsunaga Y, Serban H, Pinilla C, Bastidas RB, Rozenshteyn R, James TL, Houghten RA, Cohen FE, Prusiner SB, Burton DR (1997) A conformational transition at the N terminus of the prion protein features in formation of the scrapie isoform. J Mol Biol 273:614–622.
48. Turk E, Teplow DB, Hood LE, Prusiner SB (1988) Purification and properties of the cellular and scrapie hamster prion proteins. Eur J Biochem 176:21–30.
49. Hosszu LL, Baxter NJ, Jackson GS, Power A, Clarke AR, Waltho JP, Craven CJ, Collinge J (1999) Structural mobility of the human prion protein probed by backbone hydrogen exchange. Nat Struct Biol 6:740–743.
50. Nicholson EM, Mo H, Prusiner SB, Cohen FE, Marqusee S (2002) Differences between the prion protein and its homolog Doppel: a partially structured state with implications for scrapie formation. J Mol Biol 316:807–815.
51. Wildegger G, Liemann S, Glockshuber R (1999) Extremely rapid folding of the C-terminal domain of the prion protein without kinetic intermediates. Nat Struct Biol 6:550–553.
52. Hosszu LL, Wells MA, Jackson GS, Jones S, Batchelor M, Clarke AR, Craven CJ, Waltho JP, Collinge J (2005) Definable equilibrium states in the folding of human prion protein. Biochemistry 44:16649–16657.
53. Kuwata K, Li H, Yamada H, Legname G, Prusiner SB, Akasaka K, James TL (2002) Locally disordered conformer of the hamster prion protein: a crucial intermediate to PrPSc? Biochemistry 41:12277–12283.
54. Kundu B, Maiti NR, Jones EM, Surewicz KA, Vanik DL, Surewicz WK (2003) Nucleation-dependent conformational conversion of the y145stop variant of human prion protein: structural clues for prion propagation. Proc Natl Acad Sci USA 100:12069–12074.
55. Collinge J, Sidle KC, Meads J, Ironside J, Hill AF (1996) Molecular analysis of prion strain variation and the aetiology of 'new variant' CJD. Nature 383:685–690.
56. Kaneko K, Zulianello L, Scott M, Cooper CM, Wallace AC, James TL, Cohen FE, Prusiner SB (1997) Evidence for protein X binding to a discontinuous epitope on the cellular prion protein during scrapie prion propagation. Proc Natl Acad Sci USA 94:10069–10074.
57. Mo H, Moore RC, Cohen FE, Westaway D, Prusiner SB, Wright PE, Dyson HJ (2001) Two different neurodegenerative diseases caused by proteins with similar structures. Proc Natl Acad Sci USA 98:2352–2357.
58. Zahn R, Guntert P, von Schroetter C, Wuthrich K (2003) NMR structure of a variant human prion protein with two disulfide bridges. J Mol Biol 326:225–234.
59. Sawaya MR, Sambashivan S, Nelson R, Ivanova MI, Sievers SA, Apostol MI, Thompson MJ, Balbirnie M, Wiltzius JJ, McFarlane HT, Madsen AO, Riekel C, Eisenberg D (2007) Atomic structures of amyloid cross-beta spines reveal varied steric zippers. Nature 447: 453–457.
60. Wong BS, Wang H, Brown DR, Jones IM (1999) Selective oxidation of methionine residues in prion proteins. Biochem Biophys Res Commun 259:352–355.
61. Kay L, Keifer P, Saarinen T (1992) Pure absorption gradient enhanced heteronuclear single quantum correlation spectroscopy with improved sensitivity. J Am Chem Soc 114:10663–10665.
62. Zhang O, Kay LE, Olivier JP, Forman-Kay JD (1994) Backbone 1H and 15N resonance assignments of the N-terminal SH3 domain of drk in folded and unfolded states using enhanced-sensitivity pulsed field gradient NMR techniques. J Biomol NMR 4:845–858.

63. Bartels C, Xia T-H, Billeter M, Guntert M, Wuthrichk K (1995) The program XEASY for computer-supported NMR spectral analysis of biological macromolecules. J Biomol NMR 5:1–10.
64. Farrow NA, Muhandiram R, Singer AU, Pascal SM, Kay CM, Gish G, Shoelson SE, Pawson T, Forman-Kay JD, Kay LE (1994) Backbone dynamics of a free and phosphopeptide-complexed Src homology 2 domain studied by 15N NMR relaxation. Biochemistry 33: 5984–6003.
65. Viles JH, Duggan BM, Zaborowski E, Schwarzinger S, Huntley JJ, Kroon GJ, Dyson HJ, Wright PE (2001b) Potential bias in NMR relaxation data introduced by peak intensity analysis and curve fitting methods. J Biomol NMR 21:1–9.
66. Stone MJ, Fairbrother WJ, Palmer AG IIIrd, Reizer J, Saier MH Jr, Wright PE (1992) Backbone dynamics of the *Bacillus subtilis* glucose permease IIA domain determined from 15N NMR relaxation measurements. Biochemistry 31:4394–4406.
67. Farrow NA, Zhang O, Szabo A, Torchia DA, Kay LE (1995b) Spectral density function mapping using 15N relaxation data exclusively. J Biomol NMR 6:153–162.
68. d'Auvergne EJ, Gooley PR (2003) The use of model selection in the model-free analysis of protein dynamics. J Biomol NMR 25:25–39.